Journal of Magnetics 17(3), 210-213 (2012) http://dx.doi.org/10.4283/JMAG.2012.17.3.210

Metallic Crack Detections by Planar Inductive Coil Sensor Under AC and DC Magnetic Fields

Joonsik Lee[1], Baekil Nam[2], and Ki Hyeon Kim[1]*

[1]*Department of Physics, Yeungnam University, Gyeongsan 712-749, Korea*
[2]*Faculty of General Education, Kyungnam University, Changwon 631-701, Korea*

(Received 28 May 2012, Received in final form 25 June 2012, Accepted 25 June 2012)

To detect the surface and the opposite side cracks on iron specimen under AC and DC magnetic fields, the planar inductive coil sensors were employed. When the induced signals were measured, the planar inductive coil sensor and the magnetic field source were lifted off about 2 mm from the top surface of the specimen. AC magnetic fields and DC magnetic fields were applied to the specimens by single straight Cu coil and NdFeB permanent magnet, respectively. The detected signals at crack positions were good coincidence with those of the simulation results.

Keywords : inductive coil sensor, metallic crack, AC magnetic field, DC magnetic field, induced signal

1. Introduction

To detect the cracks of the metallic components, the nondestructive evaluation (NDE) by using the electromagnetic induction sensors has been widely employed. It has been mainly applied for inspection of metal constructions, pipes, and nuclear power plants, etc.. Among the electromagnetic based nondestructive evaluation, the induction coil probes can easily detect the induced signal due to the change of the magnetic field distribution at cracks and other defects on specimens [1, 2].

In general, the representative magnetic field sensors are SQUID, induction coil, flux gates, optically pumped magnetometers, magnetoresistive sensors and Hall sensors. Among these magnetic field sensors and applications, the inductive coil sensors have been used for positions and distance detection, magnetic recording heads, as well as nondestructive testing (NDT). These Induction coils have the good advantages for simplicity of operation and design, wide frequency bandwidth, large dynamics, and the wide detectable field range, etc.. In inductive search coil, their transfer function results from fundamental Faraday's law, the induced voltage induced from the coil can be simplified [3-7].

$$V_{signal} = -\frac{d\phi}{dt} = \frac{d(NA\mu_0\mu_r H)}{dt} \propto NAf \quad (1)$$

where, ϕ is the magnetic flux in the coil, N is the number of turns of wire, A is the effective area of the loops, μ_o is the permeability of vacuum, μ_r is the relative permeability of the core and H is the magnetic field intensity around the coil which is proportional to the operating frequency, f. From the equation (1), that high amplitude of signal from the coil can be obtained by increasing the number of turns, N of wire in the coil. However, the increasing total length of wire leads to additional resistance noise. In practice, the coil must have enough windings to ensure sufficient signal amplitude so that the performance is not impacted by amplifier noise. However, the optimization process for coil performance, in many cases, is not as easy [8].

In order to improve the signal to noise ratio, the geometrical conditions of the inductive sensors should be optimized and reduced the size by using high permeable magnetic core. Therefore, we fabricated the a few hundreds micron-scaled planar inductive coil sensor. And then the measured signals were compared with those of the simulation results, which the induced signals were detected under the AC or the DC magnetic fields applying on iron specimen, respectively.

*Corresponding author: Tel: +82-53-810-2334
Fax: +82-53-810-4616, e-mail: kee1@ynu.ac.kr

2. Experimental Procedure

The planar inductive coil sensor probe is composed of the planar inductive sensor and the magnetic field generator which is the straight single Cu coil or a cube typed permanent magnet for applying AC or DC magnetic field to the specimen.

The micro-sized planar inductive coil sensor was fabricated on AlTiC substrate (1 mm × 1 mm × 2 mm) using sputtering, electroplating and photo-lithography process, etc.. The planar inductive sensor has total 120 turns which has three layers stacked structure. The total dimension of the planar pickup coil and the cross-sectional coil dimension have 750 μm × 720 μm × 35 μm and 2 μm (w) × 4 μm (t), respectively. The $Co_{24}Ni_{37}Fe_{39}$ magnetic films were employed as a magnetic core at the bottom and the top layer of the planar coil layer, which magnetic core has a 0.8 μm-spaced gap between bottom magnetic layer (207 μm × 208 μm × 6.5 μm) and top magnetic layer (157 μm × 250 μm × 9 μm). The optical images of the fabricated planar inductive sensors are shown in Fig. 1.

To predict the induced signals using planar inductive coil sensors at crack positions, the electromagnetic simulations were performed by the finite element method using EM2D program of ANSYS and its relevant typical model was shown in Fig. 2. The artificial slit shaped cracks on magnetic iron specimen were prepared, which the 1 mm-wide slit typed cracks were varied with 0.1 mm, 0.2 mm, and 0.5 mm of the depth, respectively, as shown in Fig. 3(b). When the AC magnetic field applied to the specimen, the driving single Cu coil was generated by the alternative current with 1 A at 1 MHz. When the

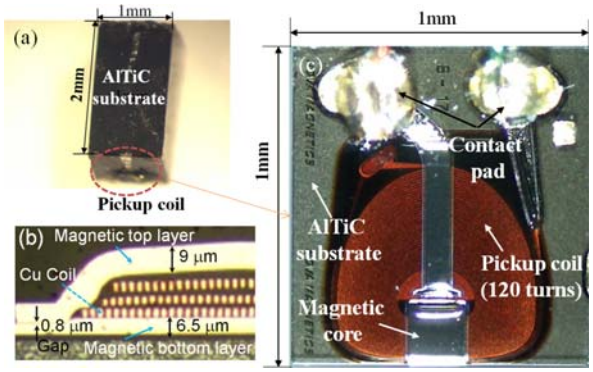

Fig. 1. (Color online) The optical image of the fabricated planar inductive coil sensor; (a) the whole view, (b) the cross sectional view and (c) the top view.

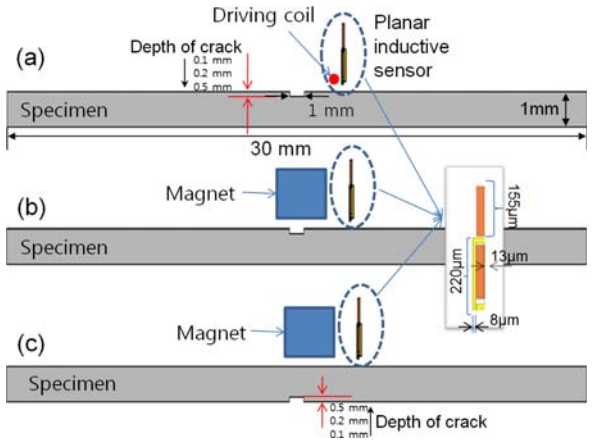

Fig. 2. (Color online) The typical schematic model for EM simulation; the surface crack detection under (a) AC and (b) DC magnetic fields and (C) the opposite side crack detection under DC magnetic fields by using the planar inductive coil sensor.

Table 1. The measuring conditions and the specifications of specimen.

Measuring conditions	Magnetic field source	AC	Cu coil (0.15 mm^2) 1 A, 1 MHz
		DC	NdFeB (7.5 × 7.5 × 6.5 mm)
	Scan speed	AC	20 mm/s
		DC	100 mm/s
	Sensor lift-off		0.2 mm
Specimen	Material		Fe
	Crack	Shape	Slit type
		Depth	0.1, 0.2, 0.5 (mm)
		Width	1 mm

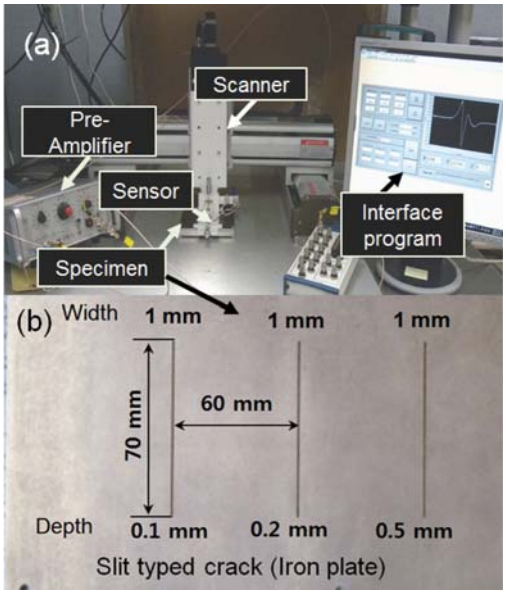

Fig. 3. (Color online) The optical images of (a) the measuring system and (b) the specimen with artificial surface cracks.

DC magnetic field applied to the specimen, the permanent magnet was employed with the magnetic field intensity of 300 Oe on simulation. In order to detect the cracks on surface and opposite side of specimen, the sensor was moved with 20 mm/s of scan speed and lift off about 2 mm from the surface of specimen, which was controlled by x, y-axis scanner. Table 1 shows the conditions of simulations and experiments under AC fields and DC fields and the specification of the specimen, respectively. The experimental crack detections are performed by using scanner with sensor probe and data acquisition system as shown in Fig. 3(a).

3. Results and Discussion

In case of the AC magnetic field applying to the specimens, it is useful for surface crack detection due to the skin depth effects with the high frequency.

On the contrary, the alternating magnetic fields are not enough to penetrate to the opposite side due to the skin depth. Therefore, we employed the DC magnetic fields using permanent magnet to detect the opposite side of crack.

Figure 4 shows the simulated results of the surface crack signals under AC and DC magnetic field and the opposite side crack signals under DC magnetic field on specimen with slit shaped artificial crack, respectively. The induced signal intensity at around surface cracks increased with the increment of the crack depth from the surface of specimen under AC and DC magnetic fields, respectively. In case of the AC magnetic field applying to the metallic specimen, although the AC magnetic field makes the eddy current on surface of specimen, the AC magnetic field is generally concentrated at the edge of crack on specimen. For the DC magnetic fields, although the magnetic fields can be distributed evenly on the specimen, it makes the strong magnetic path at the small width of crack. These are caused by the AC and DC magnetic fields concentrations on near edge side of surface cracks as shown in Fig. 5(a) and (b), respectively. And the magnetic field gradient on the edge side of the crack was increased with the increment of the depth of crack due to the increment of the flux leakage path of the magnetic fields on magnetic materials in comparison with that of air. These induced signals looked like a single peak due to the small width of crack, the resultant signals were combined two signals which were originated from each of the right and left edge side of signals. The signal intensities for the opposite side crack under DC magnetic field also increased with the increment of depth of cracks. In case

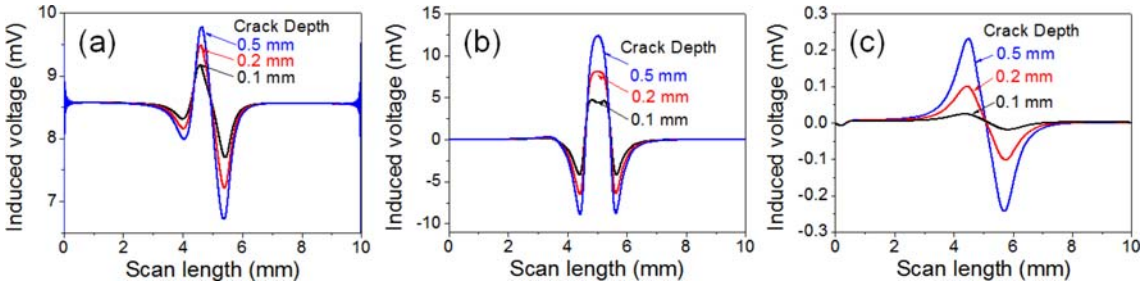

Fig. 4. (Color online) The simulated results with the increment of crack depth; (a) the surface crack signals under AC magnetic field, (b) the surface crack signals under DC magnetic field, and (c) the signals from the opposite side cracks under DC magnetic field on specimen, which signals were detected by using a planar inductive coil sensor, respectively.

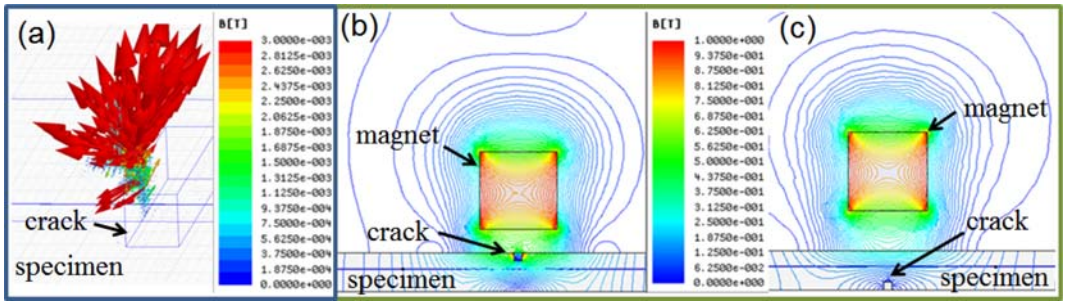

Fig. 5. (Color online) The magnetic field distributions by simulations; (a) AC magnetic fields distribution for the surface crack, (b) DC magnetic fields distribution for the surface crack and (c) DC magnetic fields distribution for the opposite side crack, respectively.

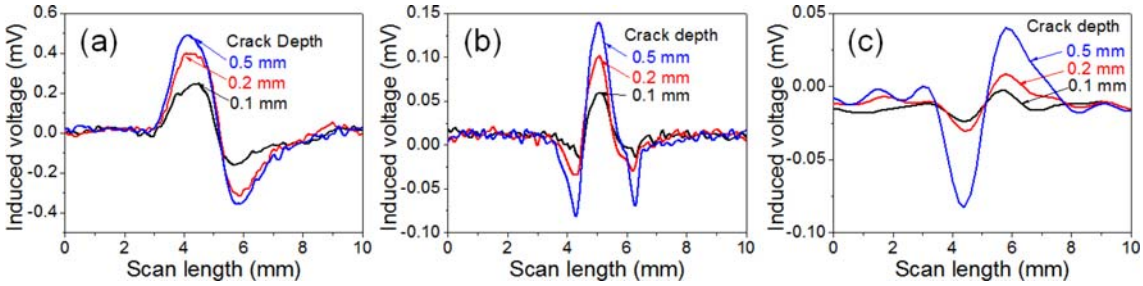

Fig. 6. (Color online) The obtained induced voltage with the increment of crack depth; (a) the signals of the surface cracks under AC magnetic field, (b) the signals of the surface cracks under DC magnetic field and (c) the signals of the opposite side cracks under DC magnetic field on the top surface of the specimens, which signals measured by using a planar inductive coil sensor, respectively.

of the opposite side crack signals, the signal shapes were not coincidence with those of the surface cracks. It reasons that the magnetic field distributions on surface area of the specimen at around the opposite side crack exhibited the relatively uniform magnetic fields distribution in comparison with that of the surface crack as shown in Fig. 5(c).

Figure 6 shows the measuring results by using a planar inductive coil sensor, which is the induced voltage with the increment of crack depth; (a) the signals of the surface crack under AC magnetic field, (b) the signals of the surface crack under DC magnetic field and (c) the signals of the opposite side crack under DC magnetic field on the top surface of the specimens, respectively. The magnitudes of the measured signals for the surface crack increase proportionally to the depth of cracks under the AC and the DC magnetic fields, respectively. In the case of the detection for the opposite side cracks under DC magnetic fields, the measured signals were exhibited the similar behaviors of the surface crack detection results. These results were good coincidence with those of the simulation results. It implies that the small size of the opposite side cracks on magnetic based metallic specimen cannot be detected under the AC magnetic fields due to the skin depth. However, the opposite side cracks can be detected under the DC magnetic fields.

4. Conclusion

The induced signals of the metallic surface and the opposite side cracks were evaluated by EM simulations and measured by the planar inductive coil sensor under AC and DC magnetic fields, respectively. The magnitudes of the induced signals of the metallic cracks were increased with the increment of the depth of cracks. The surface cracks were detected well under the AC magnetic field applying to the specimen. Under DC magnetic fields, the opposite side crack as well as the surface side crack was detected. All of the induced output signals were in good agreement with those of simulation results. As results, the micron-scaled planar inductive coil sensor probe is good applicable for the surface and the opposite side crack detections on metallic specimens under AC and DC magnetic fields, respectively.

Acknowledgement

This work was supported by the 2012 Yeungnam University Research Grant.

References

[1] O. Hesse and S. Pankratyev, Meas. Sci. Rev. **5**, 86 (2005).
[2] Yu-Jung Cha, Baekil Nam, Jongryoul Kim, and Ki Hyeon Kim, Sens. Actuators: A **162**, 13 (2010).
[3] S. Tumanski, Meas. Sci. Technol. **18**, R31 (2007).
[4] C. Cavoit, Rev. Sci. Instrum. **77**, 064703 (2006).
[5] O. Hesse and S. Pankratyev, Meas. Sci. Rev. **5**, 86 (2005).
[6] S.-H. Yoon, S.-W. Lee, Y.-H. Lee, and J.-S. Oh, Sensors **6**, 712 (2006).
[7] A. Jander, C. Smith, and R. Schneider, Proc. 10th SPIE International Symposium Nondestructive Evaluation for Health Monitoring and Diagnostics Conference **5770**, 1 (2005).
[8] R. J. Prance, T. D. Clark, and H. Prance, Encyclopedia of Sensors **10**, 1 (2006).